Operational Evaluation of a Turbulence Closure Model Forecast System

STEPHEN D. BURK AND WILLIAM T. THOMPSON

Naval Environmental Prediction Research Facility, Monterey, CA 93940

(Manuscript received 21 February 1982, in final form 16 June 1982)

ABSTRACT

A one-dimensional turbulence model has been coupled with the large-scale fields of a hemispheric model so as to produce a high-resolution marine boundary layer forecast system. Model initialization is performed either by use of individual ship soundings or from standard fields of the hemispheric model. Detailed boundary layer forecasts in specified oceanic regions are desirable for many purposes, but large-scale model forecasts with such high resolution are computationally impractical. This paper presents results from approximately 90 different 24 h forecasts at the location of four different ocean station vessels.

We statistically compare model forecast profiles of temperature and moisture with verifying soundings, and also evaluate persistence as a forecast. Results consistently show a significant improvement of the model forecasts relative to persistence. The one-way influence driving force provided by large-scale time derivative terms derived from the hemispheric model is found to be very important to this coupled forecast system.

1. Introduction

There are a great many circumstances in which reliable, high-resolution forecasts of marine atmospheric boundary layer behavior would be useful. Fog and visibility forecasts, and forecasts of atmospheric refractivity characteristics are important examples. Such forecasts are particularly difficult in data-sparse, open ocean regions. Here we describe an operational turbulent boundary layer forecast system, developed for the U.S. Navy, which addresses this problem and deals with the constraints imposed by the limitations of the operational data base.

Previous work with boundary layer turbulence models has generally involved either idealized simulations (e.g., Wyngaard *et al.*, 1974; Burk, 1977; Oliver *et al.*, 1978) or simulations using detailed, high-quality data from large research experiments (e.g., Wyngaard and Cote, 1974; Yamada and Mellor, 1975). Miyakoda and Sirutis (1977) tested the Geophysical Fluid Dynamics Laboratory's general circulation model with a boundary layer parameterization that contained a version of the Mellor and Yamada (1974) closure equations; however, as far as we are aware, there have been no previous attempts to utilize a second-moment closure model in an operational framework.

Most basic research orientated simulations with turbulence models have dealt with horizontally homogeneous situations. But a general purpose atmospheric boundary layer model which is designed to make operational forecasts cannot neglect advection. However, isolated ship soundings and the large-scale analysis and forecast fields from the Fleet Numerical Oceanography Center (FNOC) primitive equation (PE) model often comprise most of our data from sizeable oceanic regions.

The boundary layer model we use is the second-moment closure turbulence model discussed by Burk (1977, 1980). In designing this planetary boundary layer (PBL) forecast system we have coupled the high-resolution sounding information which initializes the turbulence model with information from the large-scale PE model which defines advective conditions in the ship's vicinity.

It is our intention to use the model to make high-resolution, short-range boundary layer forecasts in local marine regions based on any designated ship sounding entering the FNOC data base from ships around the globe. In order to adequately test this forecast system we have used weather station ship soundings. Our approach has generally been to make real-time 24 h forecasts at each of several weather ships, and then use the next day's ship sounding to verify the model forecast.

As an alternative mode of execution, we have also tested the feasibility of initializing the model solely based on large-scale field information, without using a ship sounding. Thus, low-resolution values from the standard levels (surface, 1000, 850, 700, 500 mb) of the FNOC PE model are interpolated to the PBL model grid initially. In this mode of operation, detailed boundary layer structure develops and evolves from the turbulence equations and the external driving forces of the large-scale fields.

This paper deals with the techniques used in developing and testing this forecast system. Section 2 describes the model and its linkage to the operational

data base. Statistical procedures and the nature of the forecast system evaluation we use are discussed in Section 3. Results from the model forecasts, and discussion of future work are presented in the final two sections.

2. Model forecast system

a. The basic PBL model

The boundary layer model we use is one-dimensional and contains 55 grid points between the surface and 3.75 km. In the terminology of Mellor and Yamada (1974), this is a level 3 model. That is, prognostic equations are integrated for temperature and moisture variance, temperature-moisture covariance, and turbulent kinetic energy. The remaining second-moment equations are solved from diagnostic relationships.

In this incompressible, Boussinesq model we solve the equations of motion for U and V; the thermodynamic equation for liquid water potential temperature θ_l; and the conservation equation for total moisture (liquid plus vapor) Q_w. Cloud physics are dealt with using the techniques developed by Sommeria and Deardorff (1977) and Mellor (1977), in which liquid water content and cloud fraction are computed based upon both mean and turbulence thermodynamic variables. Precipitation is parameterized by computing a gravitational flux of liquid water from a droplet modal radius that is computed from the mean liquid water content and an assumed droplet number density (Barker, 1977). Radiative cooling/heating rates are computed for longwave and shortwave radiation by detailed solution to the radiative transfer equation. The method developed by Oliver *et al.* (1978), which includes computation of radiative fluxes in-cloud as well as out, is used here.

b. Boundary conditions and initialization

At the model's lower boundary, similarity theory solutions are used to compute variables at the first grid point above the surface. The sea surface temperature is held fixed during the period of the forecast, its value either being given by shipboard bucket temperature measurement if available or, if not, interpolated to the ship location from the FNOC hemispheric sea surface temperature field. Surface roughness lengths are computed with Charnock's relationship,

$$z_0 = \frac{\alpha U_*^2}{g},$$

where U_* is the surface friction velocity and g the acceleration due to gravity. Garratt (1977) has shown that oceanic observations of wind stress and wind profiles are consistent with Charnock's relationship when the empirical constant α is equal to 0.0144 and von Kármán's constant κ is 0.41 ± 0.025. However, our chosen similarity profiles come from the Kansas experiment data (Businger *et al.*, 1971) and require $\kappa = 0.35$. This value of κ, in conjunction with Garratt's regression relationship between drag coefficient and wind speed, necessitates that we take $\alpha = 0.05$ in order to fit data points in Garratt's Figs. 3 and 4. We use the same roughness length for momentum, temperature and moisture.

In the stable atmosphere at the top of the grid (3.75 km), we set all turbulence variables to zero. The vertical shear of wind is set to zero there, while the temperature and moisture lapses are held fixed at the upper boundary.

Initialization of the temperature and moisture field over the entire grid takes place by linear interpolation from the mandatory and significant levels of the ship sounding and deck level measurements. Generally the grid contains higher resolution than the sounding profile. This high resolution permits development of elevated inversions and a detailed evolution of the PBL subject to boundary conditions and external, large-scale forcing.

To initialize the U and V components of the wind at each of the model's grid points we use the winds at standard pressure levels from the FNOC hemispheric model analysis. A two-dimensional field interpolation scheme is used to interpolate wind values surrounding the ship to the ship's location and to proper height. Then these components are interpolated vertically to the remainder of the PBL grid points. This same interpolation technique is used for initializing temperature and moisture profiles in those tests in which high-resolution sounding information is not utilized.

Initial values of all turbulence variables are set to zero except for turbulent kinetic energy which is initially set to a vertical distribution typical of a neutral atmosphere. We then begin a spin-up procedure in which the mean wind, temperature and moisture fields are held fixed as we iterate, but the turbulence variables are permitted to adjust to the mean profiles. This type of spin-up procedure is common in turbulence closure modeling. When the evolution of the turbulence variables has slowed because a near-equilibrium state with the fixed mean fields has been approached, we then begin marching in time and permit the mean fields to change. This spin-up period generally takes about an hour of simulation time, with $t = 0$ for the forecast being set at the end of the spin-up period.

c. Large-scale forcing

Turbulent fluxes are often weaker in the marine boundary layer than in the daytime, continental PBL. A typical ratio of inversion height to Monin-Obukhov length Z_i/L in the continental PBL is 100, while for

the marine PBL a more typical value is 10. This leads to enhanced importance of advective terms in the upper portion of the marine PBL (MPBL).

The FNOC hemisphere PE model computes synoptic changes and produces analysis and forecast fields at 12 h intervals. We use these large-scale fields to define synoptic changes occurring at the location of the boundary layer forecast. Therefore, the large-scale fields provide a coarse resolution dynamic and thermodynamic forcing which affects the detailed MPBL behavior.

Total time derivatives of the large-scale field variables, i.e.,

$$\left(\frac{D\bar{\phi}}{Dt}\right)_L = \frac{\bar{\phi}^{\tau+\Delta\tau} - \bar{\phi}^{\tau}}{\Delta\tau},$$

are computed at hemispheric model grid points in the vicinity of the PBL forecast location. Here $\bar{\phi}$ represents any one of the mean PBL model variables. The total time derivatives ("total tendencies") during the first 12 h $\Delta\tau$ of the forecast are computed from the analysis and 12 h forecast fields. During the second 12 h the 12 and 24 h large-scale fields are used for computing total tendencies. These derivatives are then interpolated to the PBL grid and added to the mean PBL equations. Note that the large-scale total temperature tendency term, for example, includes heating due to subsidence as well as horizontal advective effects and other large-scale diabatic effects.

A potential risk with this approach involves redundancy. In using a large-scale model which itself contains a boundary layer parameterization to provide forcing to our boundary layer model, we may exaggerate the effects of boundary layer processes. To avoid this problem, we use an altitude-dependent weight factor ξ in conjunction with $(d\bar{\phi}/dt)_L$. At heights above 850 mb ξ is unity, while ξ decreases to zero below 850 mb as the surface is approached, thus permitting the high-resolution closure model terms to dominate in the boundary layer. The PBL model equations for the mean variables are thus of the form

$$\frac{\partial\bar{\phi}}{\partial t} = \frac{\partial}{\partial z}(-\overline{w'\phi'}) + \xi\left(\frac{d\bar{\phi}}{dt}\right)_L,$$

where

$$\xi = \begin{cases} 1, & Z > Z_{850} \\ (Z/Z_{850})^2, & 0 < Z \leq Z_{850}. \end{cases}$$

In the free atmosphere where the turbulent flux divergences are small this technique has the desirable feature that 12 and 24 h forecasts of the large-scale PE model are reproduced.

3. Forecast verification procedure

In order to evaluate this forecast system we have utilized the regular soundings from several weather station ships. In particular, three ships in the North Atlantic are used (Fig. 1) and, before it was decommissioned, ship *Papa* in the Gulf of Alaska was used.

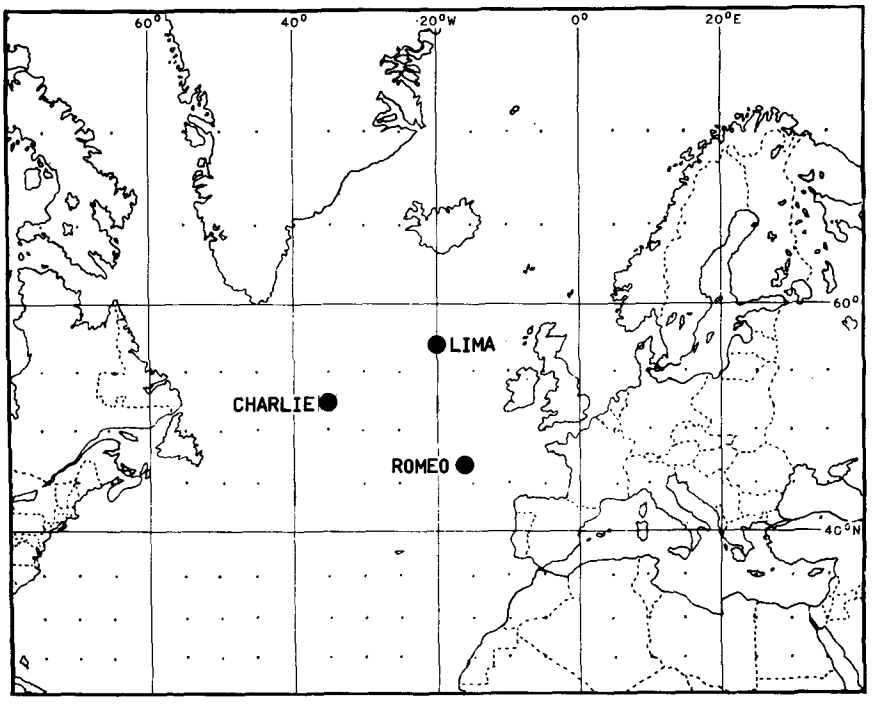

FIG. 1. Location of North Atlantic Ocean station ships whose data were used in this study.

TABLE 1. RMS 24 h forecast values (RMSF) and RMS persistence values (RMSP) for potential temperature and specific humidity at ship *Papa*.

	θ (°C)		q (g kg^{-1})	
Date	RMSF	RMSP	RMSF	RMSP
5/9	1.61	4.06	0.48	1.30
5/10	1.32	1.63	0.62	0.90
5/11	1.77	4.84	0.65	1.42
5/12	2.44	1.32	1.07	2.60
5/13	5.14	4.41	1.01	1.67
5/14	1.55	2.62	0.81	0.72
5/15	4.53	5.86	1.61	1.66
5/19	3.65	1.91	0.71	1.13
5/21	2.23	6.40	0.74	1.21
5/22	2.07	1.59	0.76	0.83
5/23	3.05	5.48	1.86	1.73
5/24	3.22	2.54	0.92	0.83
5/25	1.16	2.09	0.43	0.45
5/27	2.10	3.73	1.27	1.51
5/28	4.31	3.89	1.44	1.09
5/29	1.76	3.31	1.20	1.31
6/1	3.38	4.53	0.86	1.45
6/2	1.82	3.75	0.48	0.76
6/3	1.56	3.11	0.49	0.97
6/4	1.13	2.09	0.86	1.16
Average	2.75	3.75	0.99	1.32

Daily 24 h model forecasts are made for these ships based upon soundings received at FNOC. These 24 h forecasts are then compared against the next day's sounding. Thus, the system is tested in an operational, real-time framework. To our knowledge, no other operational model has been tested in such detail against individual radiosondes.

In order to quantitatively evaluate the validity of the forecast, we use a method which involves computing average root mean square (RMS) statistics. The average RMS error of the forecast sounding compared to the verifying sounding (RMSF) is computed, as is the same quantity for persistence compared to the verifying sounding (RMSP). These were computed as follows:

$$\text{RMSF} = \left\{\sum_{k=1}^{N} \frac{(\chi_k^f - \chi_k^v)^2}{N-1}\right\}^{1/2},$$

$$\text{RMSP} = \left\{\sum_{k=1}^{N} \frac{(\chi_k^i - \chi_k^v)^2}{N-1}\right\}^{1/2}.$$

Here χ represents the variable of interest (either temperature or specific humidity in this discussion), N the total number of PBL model grid points (55), and superscripts f, v and i represent a value from the model forecast, a value from the verifying sounding, or a value from the initial sounding, respectively.

In Table 1 the results of these RMS computations are shown for the full set of our forecasts based on ship *Papa* soundings. Also, we compute a total average of the RMS values for the period as

$$\text{Total average RMS} = \frac{1}{M}\{\sum_{j=1}^{M}(\text{RMS})_j^2\}^{1/2},$$

where M is the total number of forecasts ($M = 20$ in Table 1).

Casual examination of Table 1 reveals that the PBL model forecasts are superior overall to persistence as a forecast. To evaluate the extent of statistical significance of this apparent superiority, we have used the paired t-test. In this test, we first compute the M differences $d_1 = (\text{RMSP})_1 - (\text{RMSF})_1$, $d_2 = (\text{RMSP})_2 - (\text{RMSF})_1, \ldots, d_M = (\text{RMSP})_M - (\text{RMSF})_M$, and their mean, $\bar{d} = (d_1 + d_2 + \cdots + d_M)/M$. Next, the sample variance S_d^2 of these differences is computed as

$$S_d^2 = \frac{1}{M-1}\sum_{j=1}^{M} d_j^2 - \bar{d}^2,$$

and the test statistic formed as $t = M^{1/2}(\bar{d} - \mu)/S_d$. Here μ is the population mean which we take to be zero following the null hypothesis that the PBL forecast system is no improvement over persistence. The paired t-statistic for potential temperature from Table 1 is found to be equal to 2.95, while that for specific humidity is 3.43. Statistical tables then show that for both of these t-values we can reject the null hypothesis at a confidence level greater than 99.5%. Thus, it is highly unlikely that the superiority of the PBL forecasts shown in Table 1 is simply due to sampling error.

4. Additional model test results

a. Forecasts based on ship soundings

As shown in Table 1, the model 24 h forecast errors in temperature and specific humidity are approximately 25% smaller than the persistence forecast. This is an encouraging result, particularly given the rather data devoid location of *Papa*.

We now discuss similar RMS statistics developed from model forecasts during two different time periods during 1981 using soundings from ship *Charlie* (52.7°N, 35.5°W). The results for the first set of forecasts are shown in Table 2.

Again, the model forecast system shows considerable skill as compared with persistence, although there are only eleven forecasts in this set.

There are discontinuities in the dates in Tables 1 and 2, either because of a missing sounding, or in some cases, because other operational considerations prevented running of this forecast model. Also, it should be pointed out that a minimum amount of data quality control has gone into eliminating bad sounding points. Only gross error checks were used to throw out points. Thus, bad points (either in the initial or the verifying sounding) which are not discarded can lead to large RMS values both for the

TABLE 2. RMS 24 h forecast values (RMSF) and RMS persistence values (RMSP) for potential temperature and specific humidity at ship *Charlie*.

	θ (°C)		q (g kg^{-1})	
Date	RMSF	RMSP	RMSF	RMSP
5/12	3.08	5.03	0.77	0.76
5/15	2.97	5.49	0.72	0.24
5/18	1.00	0.78	1.46	1.40
5/21	3.54	6.04	1.92	0.59
5/22	1.29	3.82	1.06	0.58
5/23	2.58	2.54	0.45	0.45
5/24	2.43	4.99	0.64	0.93
5/25	1.36	3.15	1.06	1.48
5/26	2.99	4.76	1.89	3.98
6/1	2.62	1.13	0.58	0.87
6/5	1.00	1.03	0.41	0.97
Average	2.43	3.97	1.12	1.48

model forecast and for persistence as a forecast. Eventually we hope to develop an interactive procedure whereby an operator at a console can make the final decision on whether to retain a questionable sounding point.

In Figs. 2 and 3 we present results for the second set of forecasts based on ship *Charlie* soundings. These 18 model forecasts were made during October 1981. Fig. 2 shows the frequency distribution of RMS errors in potential temperature for the forecast model and for persistence. The paired t-statistic and associated 90–95% confidence level indicate that the near 25% improvement in model RMS skill over persistence is unlikely to be a result of sampling error. Fig. 3 shows that this PBL forecast system exhibits a skill level for forecasting specific humidity similar to that for potential temperature.

In Table 3 we summarize the results from forecasts made based on ship *Romeo* (47°N, 17°W) and ship *Lima* (57°N, 20°W). These results represent mean RMS errors for 19 different 24 h forecasts in the case of *Romeo*, and 20 forecasts for *Lima*.

Although all of the model mean errors in Table 3 are less than those given by persistence as a forecast, we see that the confidence levels for these cases are less than our previous values. In fact, in several instances we cannot reject the null hypothesis. Thus, for these ships it appears necessary to build up a larger forecast set in order to arrive at reliable conclusions concerning the apparent improvement in the PBL forecast system.

b. Forecasts based solely on large-scale fields

As mentioned previously, we have also tested this forecast system in a mode in which the PBL model is initialized solely from the large-scale FNOC fields. In order to compare results from this mode of initialization with results based on ship-sounding initialization, we have run in the large-scale initialization mode at the ship locations. This involves interpolating from the large-scale FNOC fields of temperature, moisture and wind at the standard pressure levels to the ship location following the method described in Section 2b. Thus, relatively coarse res-

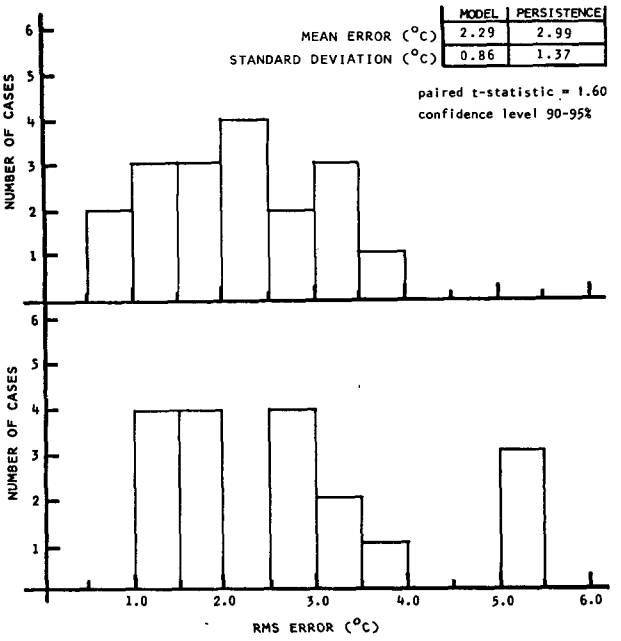

FIG. 2. Frequency distribution of RMS errors in potential temperature for 18 different 24 h forecasts initialized with ship *Charlie* soundings. Upper histogram for model forecasts, lower for persistence.

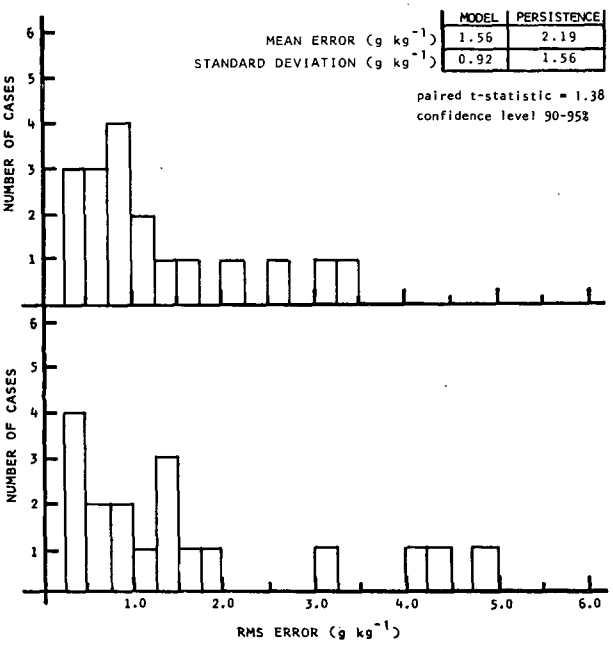

FIG. 3. As in Fig. 2, except forecasts of specific humidity.

TABLE 3. Mean model forecast and persistence RMS errors for ships *Romeo* and *Lima*. Confidence levels are based on paired *t*-tests.

	Forecast	Persistence	Confidence level
Temperature θ (°C)			
Romeo	2.93	3.78	97.5–99%
Lima	3.17	4.39	Null
Humidity q (g kg^{-1})			
Romeo	1.67	2.00	Null
Lima	1.07	1.49	95–90%

olution information is used to provide initial vertical profiles.

In this mode of operation, we also verify against coarse resolution profiles of the same type generated from the next day's analysis fields, rather than verifying against a ship sounding. Since the resolution of wind, temperature and humidity profiles is relatively coarse in this mode, the vertical profiles will tend to be smoother. It is well known that smooth fields will generally produce smaller RMS errors than more irregular fields. Thus, we may anticipate somewhat smaller RMS errors in this mode of operation as compared to the ship sounding method. But it is important to note that although we start with smooth fields, the PBL model will tend to develop a structured profile (e.g., wind shear zones, inversions) during the course of the 24 h forecast. Thus, we expect the persistence forecast to benefit the most from the fact that

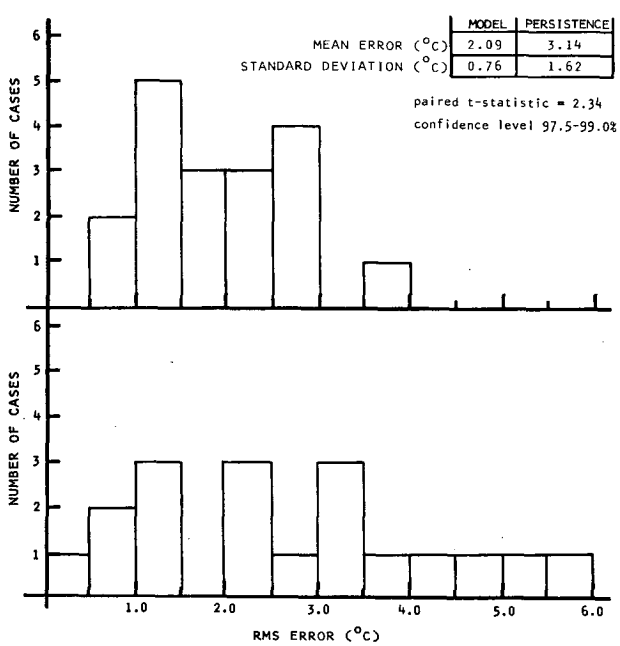

FIG. 4. Frequency distribution of RMS errors in potential temperature for 18 different 24 h forecasts initialized by large-scale field interpolation to the ship *Charlie* location. Upper histogram for model forecasts, lower for persistence.

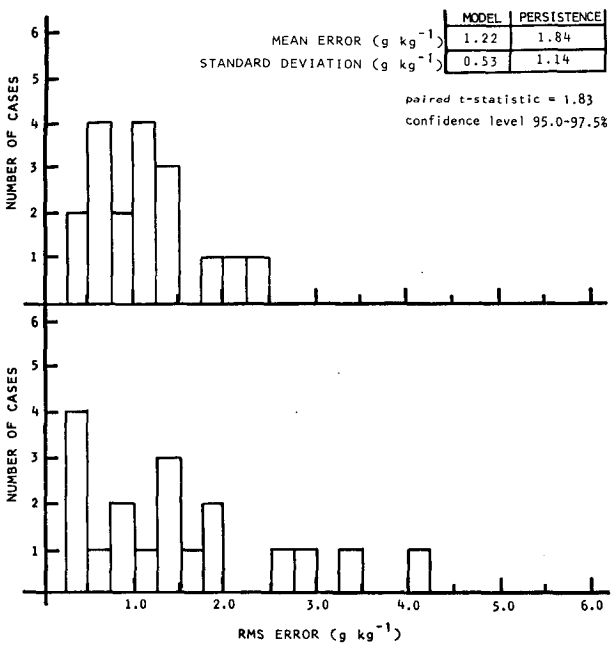

FIG. 5. As in Fig. 4, except forecasts of specific humidity.

the initial and verifying fields are smooth. Another advantage this large-scale interpolation method has over the ship sounding method is the degree of data quality control. Data in FNOC analysis fields have been subjected to considerable quality control and consistency checking. The ship sounding procedure checks only for gross errors. In any case, we will focus primarily on model forecasts versus persistence in this mode of operation, rather than comparing RMS errors here with RMS errors from the ship sounding method.

In Figs. 4 and 5 we show results from this large-scale initialization scheme for 18 forecasts made during October 1981 at the location of ship *Charlie*. The potential temperature RMS error for the PBL model forecasts is seen in Fig. 4 to be ~33% less than that of persistence, and this with a high confidence level. The RMS error results for specific humidity show this same degree of model skill (Fig. 5). If we are to consider running the forecast model operationally in this mode, freeing us from the constraints of initializing with a ship sounding, these are the type of results we must achieve.

We did not produce any forecasts at the ship *Papa* location using this mode of operation because *Papa* was deactivated before we developed this technique. In Table 4, however, are the results of 19 forecasts made at the location of ship *Romeo* and 20 forecasts at *Lima*'s location.

Again, in each category, the PBL model shows a substantial improvement over persistence, with a high confidence level that this is not due to sampling error (except for the *Lima* potential temperature forecasts).

TABLE 4. Mean model forecast and persistence RMS errors for ships *Romeo* and *Lima* using large-scale initialization.

	Forecast	Persistence	Confidence level
Temperature θ (°C)			
Romeo	2.42	3.45	>99.5%
Lima	2.43	3.53	Null
Humidity q (g kg^{-1})			
Romeo	1.35	2.00	>99.5%
Lima	0.72	1.34	90–95%

c. *Individual forecast details*

If we now examine several individual forecast cases, we can illustrate some of the advantages and some of the difficulties which this PBL model forecast system possesses. For the purpose of discussion, we select cases initialized from ship soundings, but many of the comments will be applicable to the large-scale initialization method as well.

Fig. 6 shows the initializing 0000 GMT *Papa* sounding of 14 April 1981, the 24 h PBL model forecast sounding, and the 15 April 0000 GMT verifying sounding from *Papa*. The initial sounding shows a slightly stable lapse rate between the surface and ~800 m, and a more stable lapse aloft. By examining the 24 h model forecast, we see that aloft the large-scale total temperature tendency term is yielding a cooling of ~2°C during the period of the forecast (vertical mixing contributes a negligible amount in this stable region). This cooling aloft acts to destabilize the boundary layer as a whole, and the model forecasts the development of a well-mixed boundary layer capped by an inversion at ~1.0 km. The verifying *Papa* sounding shows excellent agreement with the model forecast aloft. The development of a 1 km deep mixed layer is also evident, although the mixed layer temperature is cooler than forecast.

We next examine the following day's forecast in which the verifying sounding in Fig. 6 becomes the initializing sounding for the next 24 h forecast. In Fig. 7 we see that the model has forecast cooling aloft again, and the development of a very deep mixed layer. The 0000 GMT 16 April verifying sounding from *Papa* contains an apparent bad point aloft. As mentioned previously, such bad points are not only troublesome to subjective interpretation of our results, but also to our compilation of RMS statistics. The boundary layer does appear to have deepened, but the forecast cooling at high levels did not materialize. Some of the ambiguity arising from the bad point in the verifying sounding of Fig. 7 is removed by examining the specific humidity profiles. In Fig. 8 it is clear that a mixed layer of ~1800 m depth is present, while the model forecast was for a 2100 m deep mixed layer.

In Figs. 9 and 10 we illustrate the importance of

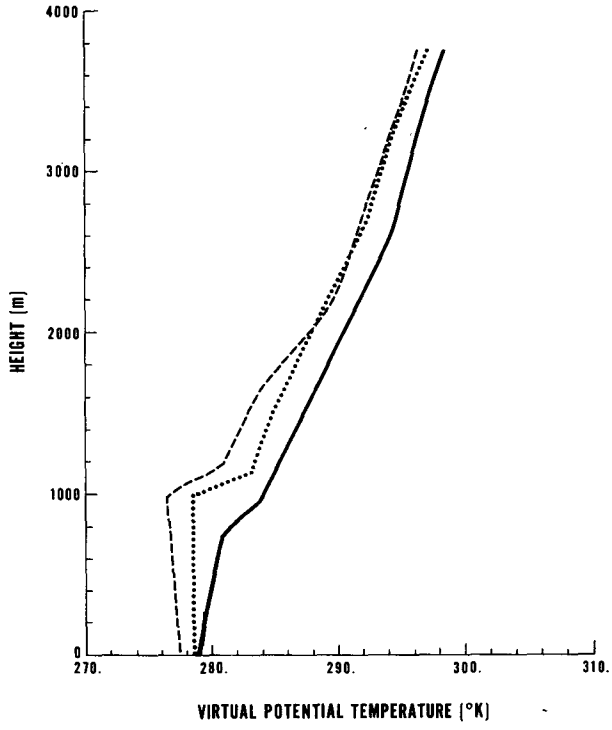

FIG. 6. Initializing ship *Papa* using 0000 GMT 14 April 81 sounding (solid); 24 h model forecast (dotted); 0000 GMT 15 April *Papa* sounding (dashed).

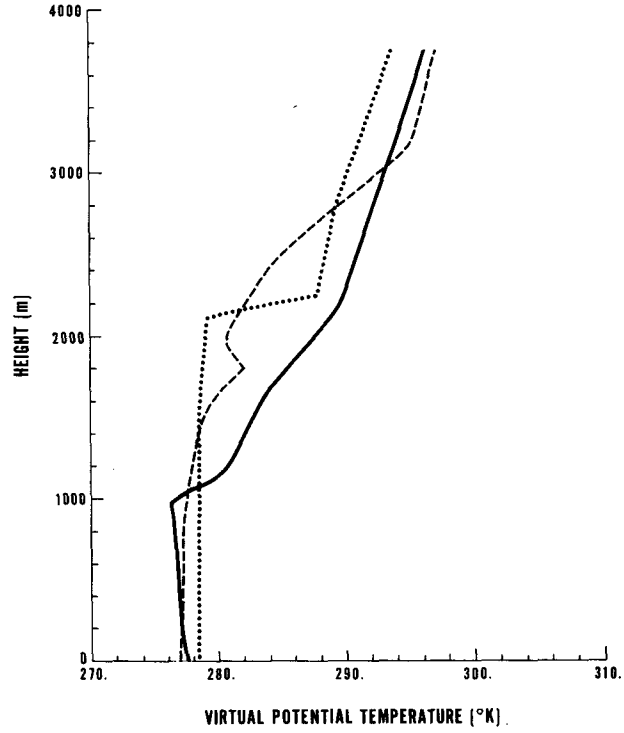

FIG. 7. Initializing ship *Papa* 0000 GMT 15 April 81 sounding (solid); 24 h model forecast (dotted); 0000 GMT 16 April *Papa* sounding (dashed).

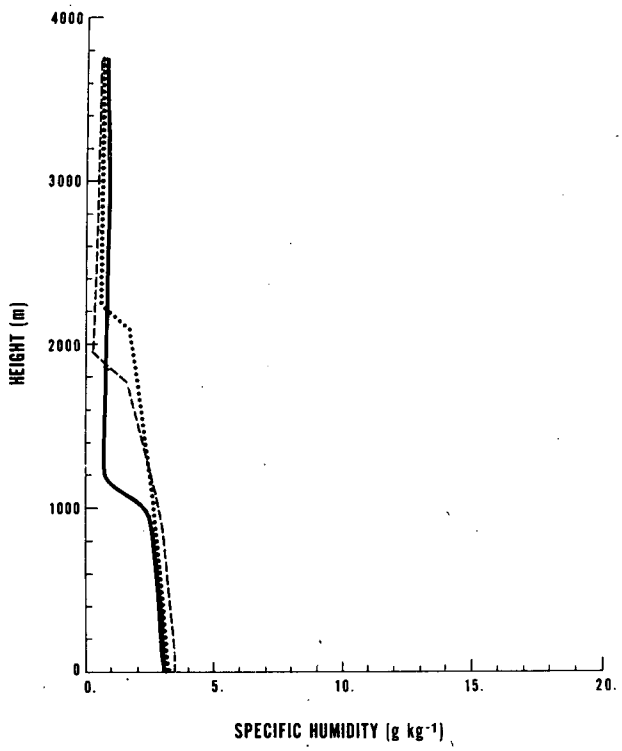

FIG. 8. As in Fig. 7 except for specific humidity.

the large-scale total tendency terms to the quality of the PBL model forecasts. Fig. 9 shows a 24 h model forecast for a case in which the tendency terms were intentionally omitted. Thus, in the stable upper regions the model forecast reduces to persistence. However, the verifying sounding in Fig. 9 looks vastly different from either the initial or the model forecast sounding. Without the inclusion of the large-scale total tendency terms, the PBL model forecast is very poor in this case.

We reran the case illustrated in Fig. 9 with the large-scale tendency terms now included. Fig. 10 shows that the model forecast is much improved with these total tendency terms. The forecast sounding does, however, show a more complex structure than the verifying sounding. The model forecasts a stratus layer capped by an inversion at ~800 m, then a second mixed layer aloft due to the destabilizing influence of the large-scale cooling.

5. Concluding remarks

This operational forecast system is designed to provide high-resolution boundary layer forecasts based on any specified ship sounding, bulk air-sea differences, and large-scale wind and tendency terms. These detailed boundary layer forecasts are important for fog and visibility forecasts, boundary layer winds, and atmospheric refractivity characteristics. We have also tested this system in a mode in which the initial fields are taken strictly from FNOC analysis fields. In either mode of operation, for a total of ~90 different 24 h forecasts, our results have consistently shown a substantial improvement over persistence. This is an encouraging result for short-range forecasts in a data-sparse environment.

The basic second-moment turbulence model used herein is one-dimensional, but its coupling with the FNOC hemispheric model provides a three-dimensional character. Further, this system seems well matched to the available open ocean data, where one often has single, high-resolution sounding data surrounded by large areas where only large-scale model information is available. While it would be desirable to have the large-scale model itself compute the PBL details, such high resolution at each grid point of a large-scale model is not yet computationally feasible.

The model produces 24 h forecasts quickly, requiring ~70 s of central processor time on a CDC CYBER-175. Another desirable feature is that the model is able to accept complex soundings directly for initialization, rather than having to be altered to fit an idealized, predetermined structure such as in the slab-type model. While such alteration of the sounding might not be difficult in persistent stratus situations on the west coast of continents where the slab structure is most applicable, for general forecasting purposes it is undesirable to always require the initial soundings to fit the slab model structure since this, by itself, can introduce a substantial RMS

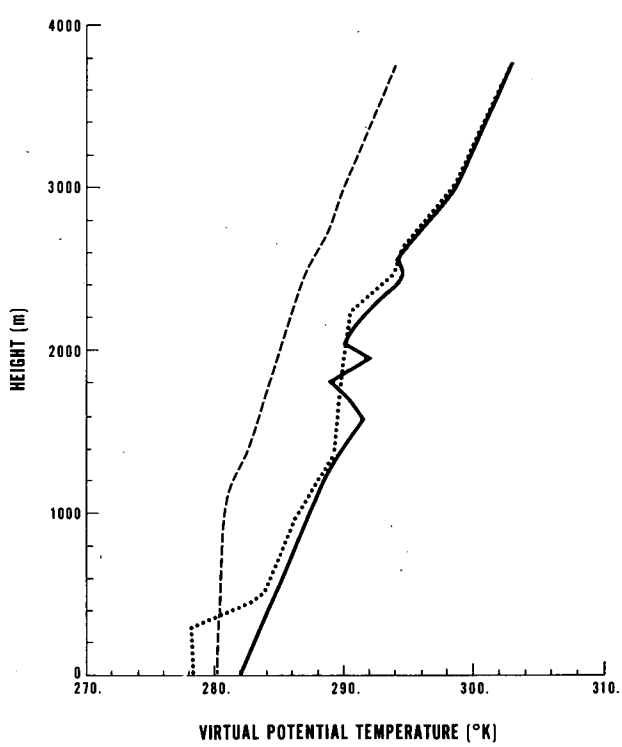

FIG. 9. Initializing ship *Papa* 0000 GMT 20 May 81 sounding (solid); 24 h forecast without tendency terms (dotted); 0000 GMT 21 May *Papa* sounding (dashed).

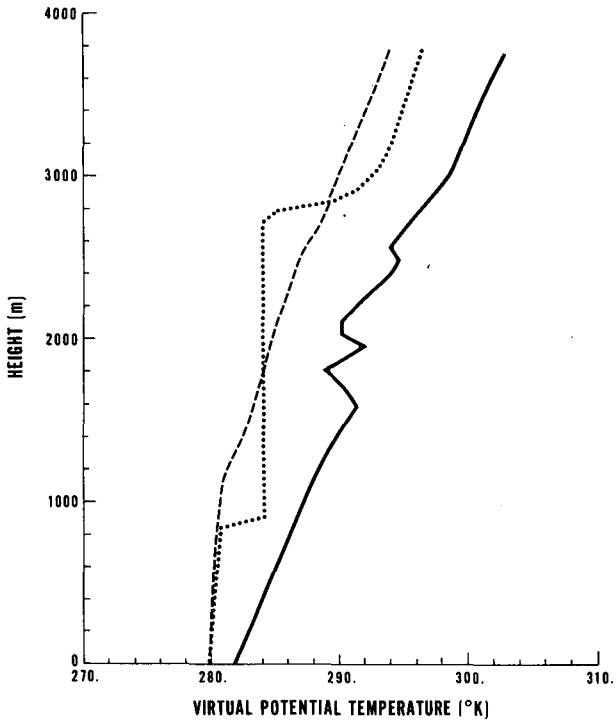

FIG. 10. As in Fig. 9 except 24 h model forecast contains large-scale tendency terms (dotted).

error. In our work with numerous soundings from the different weather ships in the Atlantic, we observed the classic slab structure (mixed layer with well-defined capping inversion) only 10–20% of the time.

Our forecast system, however, is not without its pitfalls. When we initialize using ship soundings, the model forecasts apply to the position of the initial sounding. A ship might steam a considerable distance from this point during the 24 h forecast period. To a large extent we seem to have overcome this difficulty with our large-scale interpolation mode in which the analysis fields are used to initialize the model. This frees us from the need for an initial ship sounding and permits us to select the location of the PBL forecast. We must also worry about the sensitivity of this forecast system to errors in the operational data, particularly errors in bulk air-sea differences in temperature. Thus far we have not conducted any extensive sensitivity studies of this kind.

We are currently in the process of making several changes to this model system. Until now we have computed the radiative fluxes by detailed solution to the radiative transfer equation within the PBL grid, but rather crudely parameterized the downward fluxes from above the top of the PBL grid. Now, since we typically have sounding information to much greater heights, we have designed the radiative transfer calculations to extend to 100 mb.

Another item that has been of concern is our ability to assess the source of trouble when the system produces a poor forecast because the large-scale model and the PBL model are closely linked. To remove some of this ambiguity, we have begun a program of exercising the forecast system on archived data fields at FNOC. This permits us to use analysis fields entirely (a so-called perfect prog approach) when forming the large-scale tendency terms. Thus, we can assess the faithfulness of the PBL forecasts when the large-scale fields are providing "perfect forecasts." We intend to report on these new results in the near future.

Acknowledgments. The authors are grateful to Dr. Ed Barker of the Naval Environmental Prediction Research Facility for helpful discussions, particularly concerning the use of large-scale tendency terms rather than computing individual finite-difference advective terms. Much of the coding which permits accessing of individual ship soundings in the FNOC data base and provides graphic output was developed by Pat Harr and Terry Keefer of CDC Corporation. The comments of Dr. Tetsuji Yamada and an anonymous reviewer were helpful. We also thank Steve Bishop for editing the manuscript and assisting with the graphics, and Winona Carlisle for accurate typing.

REFERENCES

Barker, E. H., 1977: A maritime boundary layer model for the prediction of fog. *Bound.-Layer Meteor.*, **11,** 267–294.

Burk, S. D., 1977: The moist boundary layer with a higher order turbulence closure model. *J. Atmos. Sci.*, **34,** 629–638.

——, 1980: Refractive index structure parameters: Time-dependent calculations using a numerical boundary layer model. *J. Appl. Meteor.*, **19,** 562–576.

Businger, J. A., J. C. Wyngaard, Y. Izumi and E. F. Bradley, 1971: Flux profile relationships in the atmospheric surface layer. *J. Atmos. Sci.*, **28,** 181–189.

Garratt, J. R., 1977: Review of drag coefficients over oceans and continents. *Mon. Wea. Rev.*, **105,** 915–929.

Mellor, G. L., 1977: The Gaussian cloud model relations. *J. Atmos. Sci.*, **34,** 356–358.

——, and T. Yamada, 1974: A hierarchy of turbulence closure models for planetary boundary layers. *J. Atmos. Sci.*, **31,** 1791–1806.

Miyakoda, K., and J. Sirutis, 1977: Comparative integrations of global models with various parameterized processes of subgrid-scale vertical transports: Description of the parameterizations. *Contrib. Atmos. Phys.*, No. 50, 445–487.

Oliver, D. A., W. S. Lewellen and G. G. Williamson, 1978: The interaction between turbulent and radiative transport in the development of fog and low-level stratus. *J. Atmos. Sci.*, **35,** 301–316.

Sommeria, G., and J. W. Deardorff, 1977: Subgrid-scale condensation in models of nonprecipitating clouds. *J. Atmos. Sci.*, **34,** 344–355.

Wyngaard, J. C., and O. R. Coté, 1974: The evolution of a convective planetary boundary layer—a higher order closure model study. *Bound.-Layer Meteor.*, **7,** 289–308.

——, O. R. Coté and K. S. Rao, 1974: Modeling the atmospheric boundary layer. *Advances in Geophysics*, Vol. 18A, Academic Press, 193–212.

Yamada, T., and G. Mellor, 1975: A simulation of the Wangara atmospheric boundary layer data. *J. Atmos. Sci.*, **32,** 2309–2329.